Taylor & Francis
Taylor & Francis Group

Phase Transitions
A Multinational Journal

ISSN: (Print) (Online) Journal homepage: https://www.tandfonline.com/loi/gpht20

Structural, optical and electrical properties of spray-deposited Fe-doped nanocrystalline $ZnS_{0.2}Se_{0.8}$ thin films

Nandkishor Manoharrao Patil, Santosh G. Nilange, Vidyadevi A. Jundale, Pratibha B. Kadam, R. Chandrashekhar & Abhijit A. Yadav

To cite this article: Nandkishor Manoharrao Patil, Santosh G. Nilange, Vidyadevi A. Jundale, Pratibha B. Kadam, R. Chandrashekhar & Abhijit A. Yadav (2021) Structural, optical and electrical properties of spray-deposited Fe-doped nanocrystalline $ZnS_{0.2}Se_{0.8}$ thin films, Phase Transitions, 94:6-8, 493-510, DOI: 10.1080/01411594.2021.1937626

To link to this article: https://doi.org/10.1080/01411594.2021.1937626

PHASE TRANSITIONS
2021, VOL. 94, NOS. 6–8, 493–510
https://doi.org/10.1080/01411594.2021.1937626

Taylor & Francis
Taylor & Francis Group

Structural, optical and electrical properties of spray-deposited Fe-doped nanocrystalline $ZnS_{0.2}Se_{0.8}$ thin films

Nandkishor Manoharrao Patil, Santosh G. Nilange, Vidyadevi A. Jundale, Pratibha B. Kadam, R. Chandrashekhar and Abhijit A. Yadav

Thin Film Physics Laboratory, Department of Physics, Electronics and Photonics, Rajarshi Shahu Mahavidyalaya, (Autonomous), Latur, MH, India

ABSTRACT

In this work, $ZnS_{0.2}Se_{0.8}$ thin films doped with Fe of various concentrations were spray deposited to investigate the influence of Fe doping concentration on the most significative structural, morphological, optical and electrical properties. An X-ray diffraction study showed that all films were polycrystalline and had a cubic zinc blende crystal structure. SEM showed that the Fe-doped $ZnS_{0.2}Se_{0.8}$ thin films had a spherical-like structure with agglomeration of grains and that their particle size was slightly increased. EDAX confirmed that the $ZnS_{0.2}Se_{0.8}$ lattice was doped with Fe. An optical study indicated that there was a direct allowed type transition. The band gap of $ZnS_{0.2}Se_{0.8}$ thin films sharply increased to 3.25 eV with Fe doping upto 0.2 mol% and then gradually decreased with increasing Fe doping concentration. DC electrical resistivity measurements confirmed that the films were semiconducting; with a minimum resistivity of 0.617×10^5 Ω-cm. Hall Effect and thermoelectric power measurements confirmed n-type conductivity.

ARTICLE HISTORY
Received 2 April 2021
Accepted 24 May 2021

KEYWORDS
Thin films; chemical spray pyrolysis; X-ray diffraction; optical properties; electrical properties; thermoelectric power

1. Introduction

In modern material science, II–VI semiconducting materials have received significant attention because of their admirable electric and optoelectronic properties and their various technological applications including photoelectrochemical (PEC) solar cells [1–5]. Zinc sulphide (ZnS) and zinc selenide (ZnSe) are II–VI semiconducting binary systems that have properties that make them suitable for optoelectronic applications [6,7]. When ZnS and ZnSe are combined, ternary zinc sulphoselenide (ZnSSe) heterostructures can be obtained. Such ternary semiconductors have been studied widely because of the possibility of tuning their characteristics significantly, including the optical bandgap (2.70–3.67 eV), lattice constant and electrical properties, simply by changing the S/Se ratio and make them useful for the device fabrication [8–10]. The two key properties of ZnS_xSe_{1-x}, which are abundant in the earth's crust, are the wide bandgap (wider than that of CdS) and low toxicity. These properties make them more attractive than the conventional toxic CdS for use as buffer layers in $Cu(In,Ga)Se_2$ (CIGS) thin-film solar cells [11,12]. ZnSSe thin films are the most suitable films for several optoelectronic and optical applications including visible laser diodes, light-emitting diodes, light emitters, solar cells and wavelength-tunable UV photodetectors [13–17].

The performance of various devices fabricated using the semiconductor materials strongly depends on the optical, electrical and PEC properties of semiconducting materials. The mentioned

CONTACT Abhijit A. Yadav aay_physics@yahoo.co.in

properties of the binary and ternary semiconducting materials can be easily tuned or adjusted (improved) through doping treatment for many potential applications [18–21]. A survey of the literature shows that mostly ions of transition metals such as Ni, Co, Cu, Fe and Cr are used for doping II–VI semiconductors [22,23].

Lohar and colleagues [24] have studied effect of Fe^{3+} (transition metal) doping on the PEC properties of ZnSe nanoparticles and hollow spheres deposited using the potentiostatic mode of electrodeposition. They reported that the pure ZnSe thin film PEC cell performance enhanced due to Fe^{3+} dopant and its efficiency increased to 0.21% from 0.07%.

Bhuse et al. [25] have studied the effect of indium doping on the PEC properties of pure $Cd_{0.6}Hg_{0.4}Se$ thin films prepared via CBD method. They observed enhancement in various PEC parameters of $Cd_{0.6}Hg_{0.4}Se$ thin films such as Voc, Isc, Fill factor and the photon-to-electrical conversion efficiency due to indium impurity.

Yellaiah and co-workers [21] used co-precipitation method to prepare pure and samarium doped $Cd_{0.8}Zn_{0.2}S$ powders and reported influence of samarium doping on the properties of the pure $Cd_{0.8}Zn_{0.2}S$ samples such as structural, elemental, optical and vibrational.

The various physical and chemical methods used to synthesize ZnS, ZnSe and ZnSSe thin films include thermal evaporation [26,27], dc magnetron sputtering [28], molecular beam epitaxy [29], screen printing [30], brush plating [31], co-precipitation [32], quasi-closed volume technique [33], close-spaced evaporation [11], chemical bath deposition [14, 34], aerosol-assisted chemical vapor deposition [35] and chemical spray pyrolysis [36]. The last is the method used most commonly for producing high-quality semiconducting thin films suitable for photovoltaic applications. This method has a number of benefits: it is simple; loss of the precursor solution to the surroundings is minimum, affordable, well control of film thickness, easy to carry out and does not need a vacuum system or high-quality substrates or chemicals. Substrates of large area and uniform layers can be deposited, and doping is very easy [37,38]. Further, spray pyrolysis produces high-quality thin films that are, uniform, pinhole-free and strongly adherent to the surface of the substrate [39,40].

Previously the growth and characterization of ZnS_xSe_{1-x} thin films using spray pyrolysis has been reported [41]. ZnS_xSe_{1-x} thin films are polycrystalline, with a cubic zinc blende structure and a preferential (111) orientation. Solid solution formation takes place with the crystallite size in the range 18–28 nm. The optical bandgap increased from 2.84 to 3.57 eV when the composition of the ZnS_xSe_{1-x} was changed. Also, the PEC properties of spray-deposited ZnS_xSe_{1-x} thin films with different values of 'x' have been studied and the maximum photo conversion efficiency (1.27%) can be achieved at $x = 0.2$ [42]. This conversion efficiency was very small because of the high resistivity of the photoelectrode material [43]. For this reason, it became necessary to decrease the resistivity of the $ZnS_{0.2}Se_{0.8}$ and improve the efficiency of the PEC cell. One of the ways of reducing the resistivity was to dope the $ZnS_{0.2}Se_{0.8}$ thin films with a suitable donor impurity and enhancing its conductivity. The effect of such dopants on $ZnS_{0.2}Se_{0.8}$ thin films is an important aspect to study. Trivalent Fe has been found to be a useful low-cost dopant because of its interesting optoelectronic properties [44–46].

The main purpose of the current study was to deposit nanocrystalline Fe-doped $ZnS_{0.2}Se_{0.8}$ thin films through chemical spray pyrolysis. The influence of Fe doping (0.05–1.00 mol%) on the structural, morphological, optical, electrical and thermoelectrical properties of spray-deposited $ZnS_{0.2}Se_{0.8}$ thin films was studied and the Fe concentration at which $ZnS_{0.2}Se_{0.8}$ thin films shows enhanced properties are reported here.

2. Experimental details

2.1 Synthesis of $ZnS_{0.2}Se_{0.8}$ and Fe-doped $ZnS_{0.2}Se_{0.8}$ thin films

The spray pyrolysis procedures that were used to deposit the $ZnS_{0.2}Se_{0.8}$ thin films have been described previously [41]. Equimolar (0.05 M) aqueous solutions of zinc chloride ($ZnCl_2$),

thiourea ($(NH_2)_2CS$), selenourea ($(NH_2)_2CSe$) and ferric chloride hexahydrate ($FeCl_3.6H_2O$) of various concentrations (0.05, 0.10, 0.20, 0.25, 0.30, 0.50 and 1.00 mol %) were used as the starting materials. The ferric chloride hexahydrate was used as a Fe^{3+} dopant. Amorphous glass slides (7.5 cm×2.5 cm×0.135 cm; Blue Star Polar Industrial Corporation, Mumbai) were used as the substrates. The films were deposited under the optimized preparative parameters mentioned in Table 1. After deposition, the thin films were allowed to cool naturally at room temperature. The adhesion of the prepared films onto the substrate was good as verified using a simple Scotch tape test.

2.2 Characterization of $ZnS_{0.2}Se_{0.8}$ and Fe-doped $ZnS_{0.2}Se_{0.8}$ thin films

As-deposited $ZnS_{0.2}Se_{0.8}$ and Fe-doped $ZnS_{0.2}Se_{0.8}$ thin films were characterized using various techniques for their structural, morphological, compositional, optical, electrical and thermoelectrical properties. The structural properties of the thin films were studied using a Philips (PW 3710) X-Ray diffractometer with Cu-Kα radiation (λ=1.5406 Å) and 2θ in the range 20–80°. Surface morphology measurements were made and compositional analysis carried out using a FEI Quanta 200 ESEM scanning electron microscope (SEM) and an Octane plus EDX Energy-dispersive X-ray spectroscopy. The optical absorption spectra of the thin films were investigated within the wavelength range 320–990 nm using a JAZ-EL200-XR1 UV–Vis spectrophotometer (JAZ, Ocean Optics Inc., USA). DC resistivity and thermoelectrical measurements were made with a Keithley Source Meter (model 2450) using a standard two-probe method. The Van-der Paw technique was used for Hall Effect measurements. Silver paste was applied to well-grown $ZnS_{0.2}Se_{0.8}$ and Fe-doped $ZnS_{0.2}Se_{0.8}$ thin films in a two-bar pattern to ensure good ohmic contacts.

3. Results and discussion

3.1 Thickness measurements

The thicknesses of the undoped and Fe-doped $ZnS_{0.2}Se_{0.8}$ thin films were measured with a sensitive Radwag microbalance using the familiar gravimetric weight difference method, making assumptions about the bulk densities (ρ) of the corresponding materials. The thickness is obtained by using the formula [47],

$$t = \frac{\Delta m}{\rho \times A} \tag{1}$$

$$\Delta m = m_1 - m_2 \tag{2}$$

where t is film thickness, Δm is mass of the film material, A is area of the film, m_1 is mass of the substrate with film, and m_2 is mass of the substrate without film. In order to get more accurate

Table 1. Optimized preparative parameters for deposition of $ZnS_{0.2}Se_{0.8}$ and Fe-doped $ZnS_{0.2}Se_{0.8}$ thin films.

Preparative parameter	Optimized values
Substrate temperature (°C)	275
Nozzle (type)	Glass
Substrate to nozzle distance (cm)	30
Carrier gas	air
Carrier gas pressure (N/m^2 or Pa)	176,520
Total deposition time (min)	13–14
Solution flow rate (cc min^{-1})	3
Molarity (M)	0.05
Substrates (type)	Soda lime glass
Dopant	Iron ($FeCl_3.6H_2O$)

results, thickness is measured using the films with maximum area. The thickness of Fe-doped $ZnS_{0.2}Se_{0.8}$ thin films doped with 0.05, 0.10, 0.20, 0.25, 0.30, 0.50 and 1.00 mol % concentrations were found to be equal to 280, 285, 294, 302, 311, 321 and 330 nm respectively.

3.2 X-ray Diffraction (XRD) studies

XRD, an easy technique, was used to confirm and determine the crystal structures of the undoped and Fe-doped $ZnS_{0.2}Se_{0.8}$ thin films. Figure 1 exhibits typical XRD patterns of undoped and Fe-doped $ZnS_{0.2}Se_{0.8}$ thin films spray deposited with Fe of various doping concentrations. ZnS and ZnSe exist in two main crystalline forms, wurtzite (hexagonal) and zinc blende (cubic). It was seen that the films were polycrystalline. A good match of the observed and standard 'd' values (Table 2) of the (hkl) planes confirmed that the films had a cubic (zinc blende) crystal structure as described in JCPDS data cards 80-0022 and 80-0021 [48, 49]. The appearance of the (111), (220) and (311) planes also reveal a cubic (zinc blende) crystal structure. Identical planes and a cubic crystal structure were also observed in previous work [50, 51].

All the XRD patterns of the Fe-doped $ZnS_{0.2}Se_{0.8}$ were found to match those of the undoped $ZnS_{0.2}Se_{0.8}$, without additional peaks (i.e. crystalline impurities) which shows that Fe does not affect its crystal structure. It also shows the films have a preferential orientation along the (111). The intensity of the (111) peak rises significantly with increasing Fe doping concentration up to 0.20 mol%. When the Fe doping concentration is increased above 0.20 mol%, there is a slight fall in the intensity of the XRD peaks. The fall in (111) peak intensity after 0.20 mol% Fe doping might be due the change in electron density or might be due to point defects created due to doping. On the other hand, there is no evidence of any considerable change in the diffraction peak position (2θ) of the Fe-doped $ZnS_{0.2}Se_{0.8}$ thin films compared with that of the undoped $ZnS_{0.2}Se_{0.8}$. A very small peak shift, apparently owing to the existence of Fe ions in the $ZnS_{0.2}Se_{0.8}$ lattice, was observed [52]. The significant change in intensity and minor change in the peak position arise due to the replacement of Zn^{2+} atoms by Fe^{3+} [53].

The lattice parameter 'a' of the cubic phase was calculated using the standard formula.

$$\frac{1}{d^2} = \frac{h^2 + k^2 + l^2}{a^2} \tag{3}$$

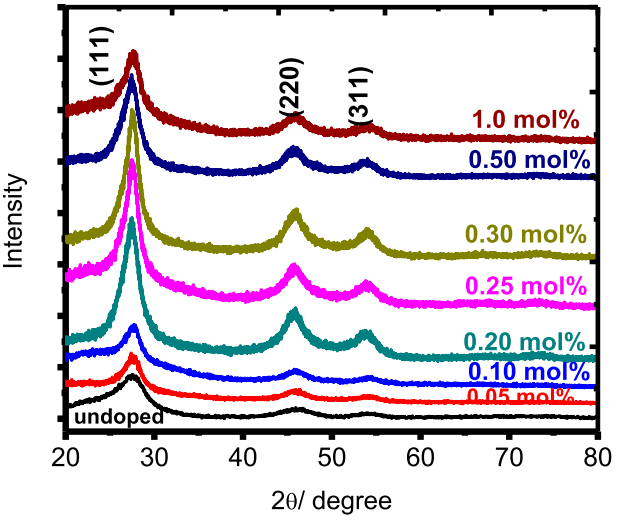

Figure 1. XRD patterns of spray deposited Fe doped $ZnS_{0.2}Se_{0.8}$ thin films.

Table 2. Various structural parameters of spray deposited $ZnS_{0.2}Se_{0.8}$ and Fe-doped $ZnS_{0.2}Se_{0.8}$ thin films.

Fe doping Concentration (mol%)	2θ (°)	d (Å)		hkl	a (Å)	FWHM (radian)	Crystallite Size D (nm)
		Observed	Standard				
Undoped	27.42	3.250	3.212	111	5.586	0.005345	28
	45.74	1.982	1.967	220			
	53.57	1.709	1.677	311			
0.05	27.39	3.253	3.212	111	5.633	0.004989	30
	45.72	1.983	1.967	220			
	53.68	1.706	1.677	311			
0.1	27.43	3.249	3.212	111	5.618	0.004677	32
	45.69	1.984	1.967	220			
	54.10	1.694	1.677	311			
0.2	27.37	3.256	3.212	111	5.643	0.004277	35
	45.67	1.985	1.967	220			
	53.48	1.712	1.677	311			
0.25	27.38	3.254	3.212	111	5.638	0.004536	33
	45.52	1.991	1.967	220			
	53.80	1.702	1.677	311			
0.3	27.44	3.247	3.212	111	5.627	0.004828	31
	45.67	1.985	1.967	220			
	53.84	1.701	1.677	311			
0.5	27.43	3.249	3.212	111	5.626	0.005161	29
	45.56	1.989	1.967	220			
	54.03	1.696	1.677	311			
1	27.59	3.230	3.212	111	5.601	0.005541	27
	45.82	1.979	1.967	220			
	54.15	1.692	1.677	311			

In this relation, *h*, *k*, and *l* are the Miller indices, and *d* is the interplanar spacing between the atoms, determined using the well-known Bragg's equation (nλ=2dsinθ). The variations of the lattice constant with Fe doping concentration are given in Table 2. The lattice constant was the maximum (5.643 Å) for $ZnS_{0.2}Se_{0.8}$ films with 0.2 mol% Fe doping concentration.

The crystallite sizes, D, of the undoped and Fe-doped $ZnS_{0.2}Se_{0.8}$ thin films were obtained from the full-width at half-maximum (FWHM) β values using Debye Scherrer's formula [30],

$$D = \frac{k\lambda}{\beta\cos\theta} \tag{4}$$

where *k* is Scherrer's constant and varies from 0.89 to 1.39. In most cases its value is close to 1. Hence it was taken as 1, λ is the wavelength of the X-ray source used (λ=0.15406 nm), and θ denotes the Bragg or diffraction angle.

The XRD peaks of the samples are considerably broadened because of the particle size effect. XRD analysis of the films indicates that the films have a cubic phase with a preferential orientation along the (111) plane. The FWHM values and crystallite sizes are shown in Table 2. The crystallite sizes of the $ZnS_{0.2}Se_{0.8}$ and Fe-doped (0.05, 0.10, 0.20, 0.25, 0.30, 0.50 and 1.00 mol%) $ZnS_{0.2}Se_{0.8}$ thin films are 28, 30, 32, 35, 33, 31, 29 and 27 nm, respectively. Clearly, the 0.20 mol% Fe-doped $ZnS_{0.2}Se_{0.8}$ thin film has the greatest crystallite size. It was seen that the crystallite size of the $ZnS_{0.2}Se_{0.8}$ thin films increased from 28 nm (undoped) to 35 nm (for 0.20 mol% Fe-doped $ZnS_{0.2}Se_{0.8}$). When the Fe doping is increased further, the crystallite size drops to 27 nm.

The preferential growth of undoped and Fe-doped $ZnS_{0.2}Se_{0.8}$ thin films was evaluated through the texture coefficient T_C(hkl) [54]:

$$T_c(\text{hkl}) = \frac{I(\text{hkl})/I_0(\text{hkl})}{(1/N)(\sum_N I(\text{hkl})/I_0(\text{hkl})} \tag{5}$$

Here T_c(hkl) is the texture coefficient of the (hkl) plane, I(hkl) is the measured relative intensity, I_0

(hkl) represents the JCPDS data card intensity of the (hkl) plane and N denotes the number of diffraction peaks. The variations of the texture coefficient along the (111), (220) and (311) planes with Fe doping concentration in the $ZnS_{0.2}Se_{0.8}$ thin films are shown in Figure 2. From Figure 2, it is clear that for the (111) plane the texture coefficient surges when the Fe concentration increases from 0 to 0.20 mol%. The low value of the texture coefficient indicates that the crystallinity of the thin films was poor. The crystallinity was boosted when the Fe doping concentration was increased from 0 mol% (undoped) to 0.20 mol%. When the Fe doping concentration is increased above 0.20 mol %, there is a slight fall in the texture coefficient. Obviously, the crystallinity of the films deposited with a 0.20 mol% Fe doping concentration is superior. The lower texture coefficient values of the (220) and (311) planes as compared with the (111) plane confirm the strong crystalline orientation of the films along the (111) plane. The larger crystallite size and texture coefficient values are due to the addition of Fe in $ZnS_{0.2}Se_{0.8}$.

3.3 Surface morphological and compositional studies

SEM was used to study the surface morphology of the undoped and Fe-doped $ZnS_{0.2}Se_{0.8}$ thin films. Figure 3 shows SEM images (magnification 40,000×) of thin films doped with Fe of various concentrations: (a) undoped, (b) 0.10 mol%, (c) 0.20 mol%, (d) 0.30 mol%, and (e) 1.0 mol %. The undoped $ZnS_{0.2}Se_{0.8}$ thin films and the films doped with Fe of 0.10 mol% had small crystallites of the same shape and dimensions. The films doped with 0.20, 0.30 and 1.0 mol% Fe had a spherical-like structure, with agglomeration of grains and a slightly greater particle size. Kumar et al. [55] observed similar morphology in electrochemically deposited Eu-, Sm- and Gd-doped ZnSe thin films.

The undoped and Fe-doped $ZnS_{0.2}Se_{0.8}$ thin films were subjected to compositional analysis through Energy-dispersive X-ray spectroscopy measurements. Figure 4 shows the EDS spectra of thin films doped with Fe of various doping concentrations: (a) undoped, (b) 0.10 mol%, (c) 0.20 mol%, (d) 0.30 mol% and (e) 1.0 mol%. The Energy-dispersive X-ray spectroscopy measurements and the atomic percentages of Zn, S, Se and Fe in the thin films are presented in Table 3. The Energy-dispersive X-ray spectroscopy studies show that all the films were nearly stoichiometric and traces of Fe indicates doping of Fe in $ZnS_{0.2}Se_{0.8}$ lattice.

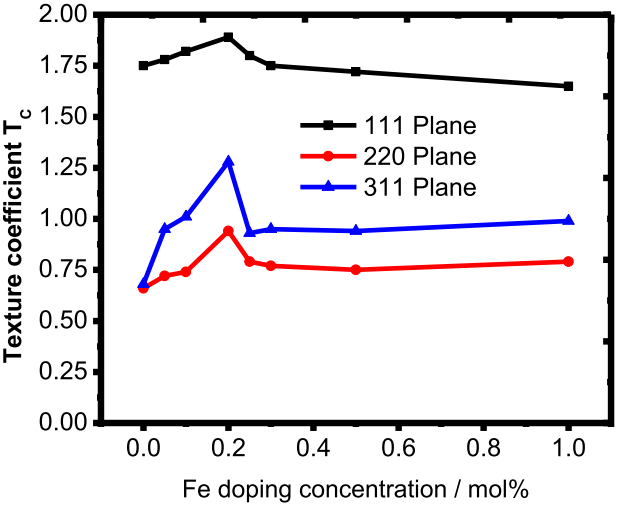

Figure 2. Variation of texture coefficient along the plane with Fe doping concentration for spray deposited Fe doped $ZnS_{0.2}Se_{0.8}$ thin films.

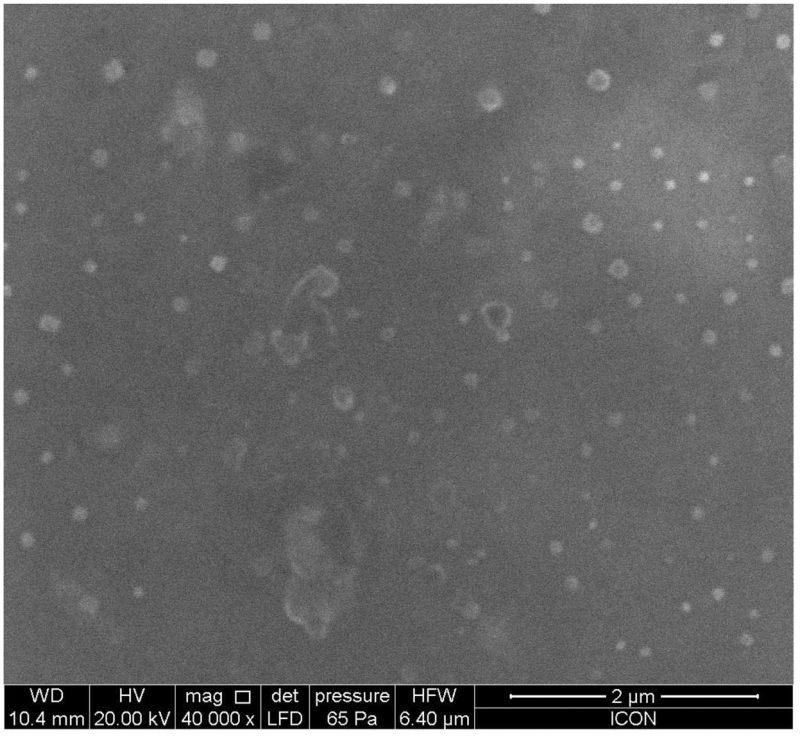

(a)

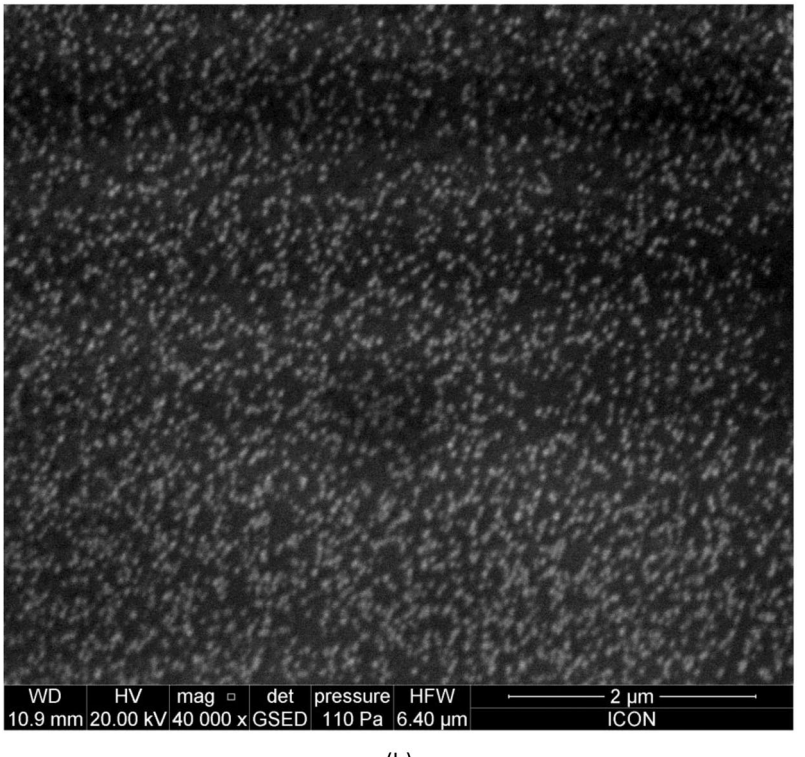

(b)

Figure 3. SEM images (magnification 40,000 ×) of Fe doped $ZnS_{0.2}Se_{0.8}$ thin films with various Fe doping concentration (a) undoped, (b) 0.10 mol%, (c) 0.20 mol%, (d) 0.30 mol%, and (e) 1.0 mol%, respectively.

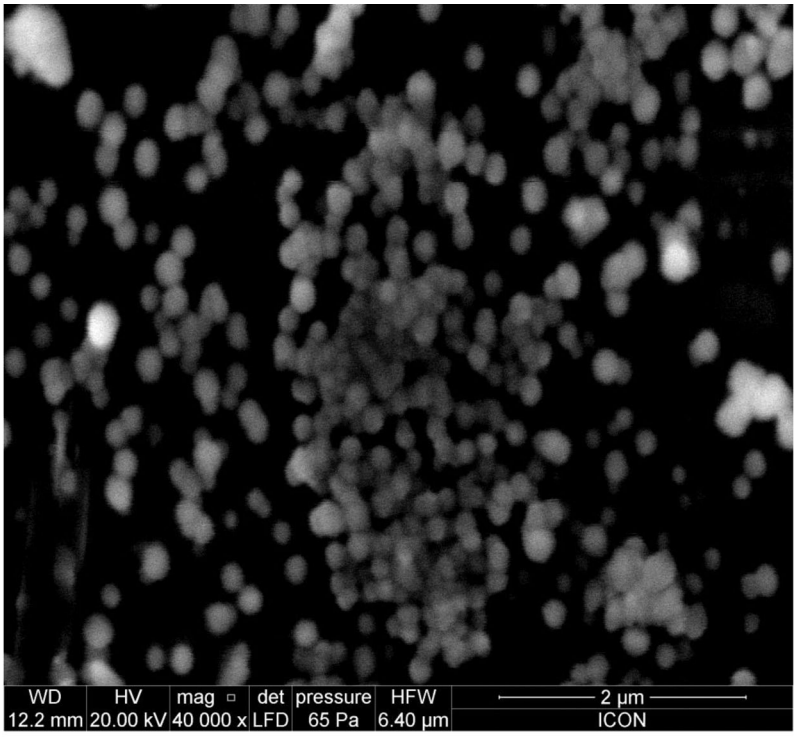

(c)

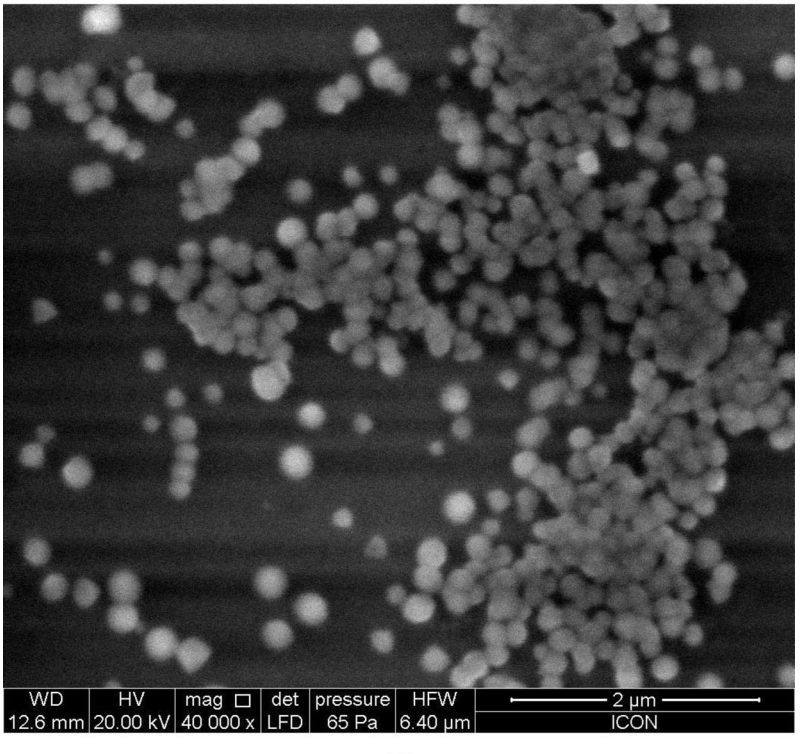

(d)

Figure 3 *Continued*

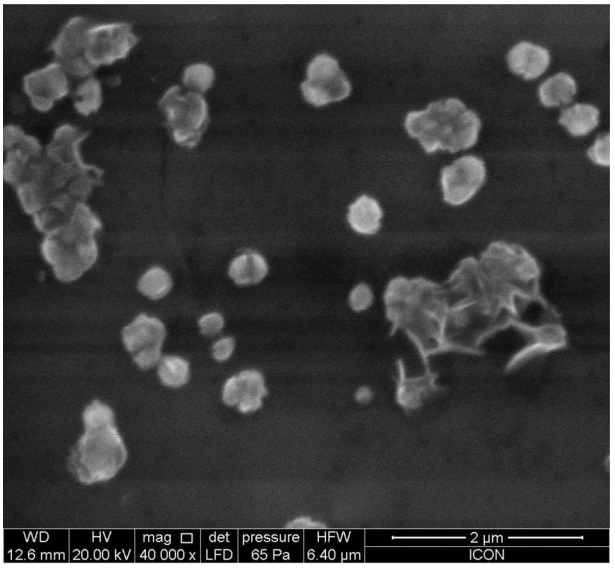

(e)

Figure 3 *Continued*

Table 3. Elemental composition of spray deposited $ZnS_{0.2}Se_{0.8}$ and Fe-doped $ZnS_{0.2}Se_{0.8}$ thin films.

	Initial composition in spraying solution (%)				Atomic percentage in film by EDS analysis (%)			
Composition	Zn	S	Se	Fe	Zn	S	Se	Fe
Undoped $ZnS_{0.2}Se_{0.8}$	50.0	10.0	40.0	0.0	50.10	9.50	40.40	0.00
0.10 mol% $ZnS_{0.2}Se_{0.8}$	50.0	10.0	40.0	0.1	49.81	9.57	40.47	0.15
0.20 mol% $ZnS_{0.2}Se_{0.8}$	50.0	10.0	40.0	0.2	49.58	9.81	40.35	0.26
0.30 mol% $ZnS_{0.2}Se_{0.8}$	50.0	10.0	40.0	0.3	49.44	9.67	40.52	0.37
1.0 mol% $ZnS_{0.2}Se_{0.8}$	50.0	10.0	40.0	1.0	48.78	9.43	40.81	0.98

3.4 Optical studies

The measurement of optical absorption spectra using UV–Vis spectrophotometer is a powerful and non-destructive technique used to study the optical properties of semiconducting nanomaterials. The optical spectra of the undoped and Fe-doped $ZnS_{0.2}Se_{0.8}$ thin films were obtained without accounting for the reflection and transmission losses in the wavelength range 320-990 nm at room temperature. Figure 5(a) shows the optical absorption spectrum of undoped and Fe-doped $ZnS_{0.2}Se_{0.8}$ thin films. It is clearly seen from the spectra that the undoped and Fe-doped $ZnS_{0.2}Se_{0.8}$ thin films have sharp absorption and the absorption edge initially slightly shifting near the lower wavelength indicating the increase of optical bandgap up to 0.20 mol% Fe doping concentration. After 0.20 mol% Fe doping concentration the absorption edge shifts towards the longer wavelength. The optical bandgap energy of the semiconductors and the nature of the transition involved (direct or indirect) in the absorption process were determined using Tauc's equation [30, 33]:

$$\alpha h\upsilon = A(h\upsilon - Eg)^n \tag{6}$$

Here Eg, α, A and $h\upsilon$ (hc/λ) denote the separation between the valence and conduction bands, absorption coefficient, absorption constant and the photon energy, respectively. The exponent n is characteristic of the transition, and its values for allowed direct, allowed indirect and forbidden

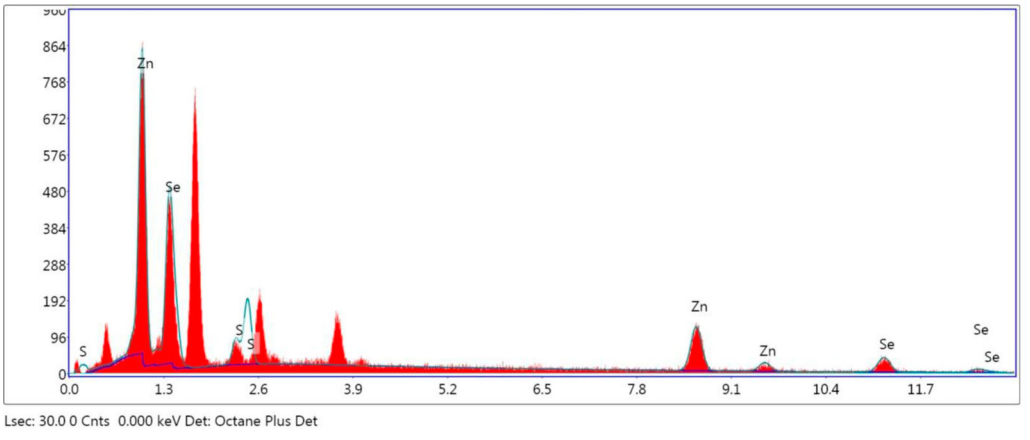

(a)

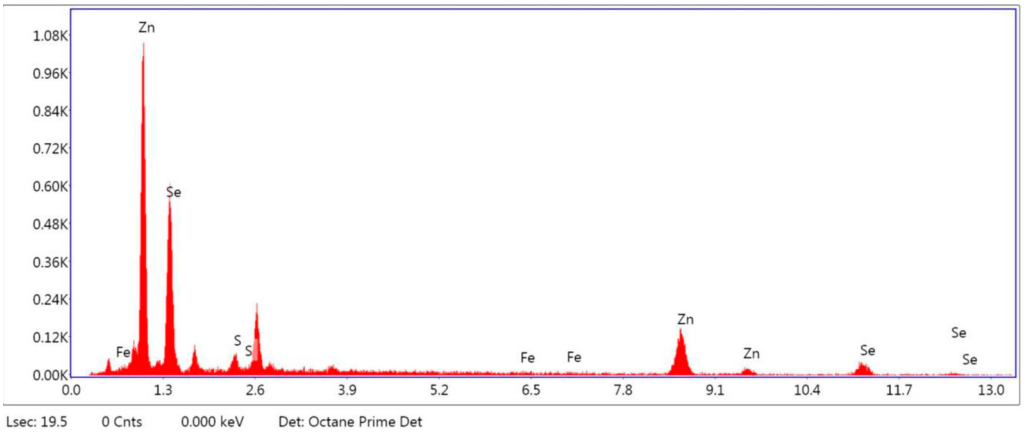

(b)

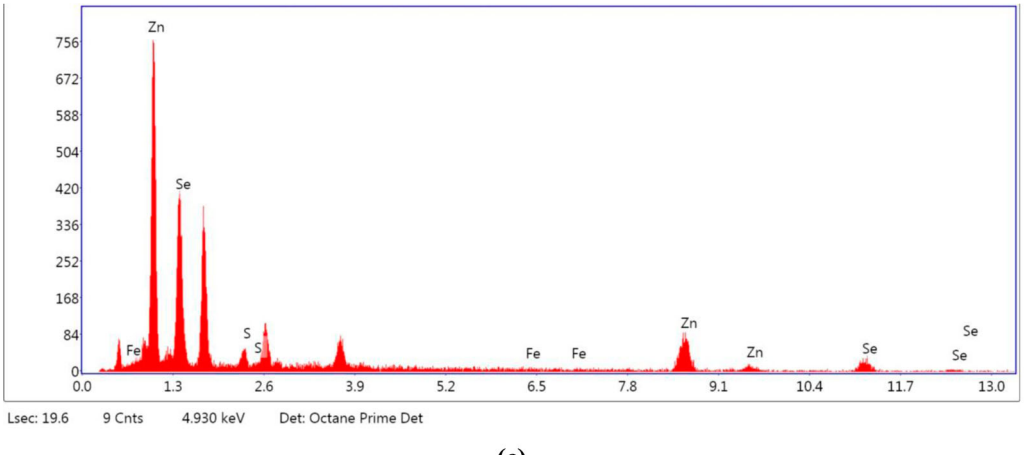

(c)

Figure 4. EDS spectra of (a) undoped, (b) 0.10 mol%, (c) 0.20 mol%, (d) 0.30 mol%, and (e) 1.0 mol%, Fe doped $ZnS_{0.2}Se_{0.8}$ thin films respectively.

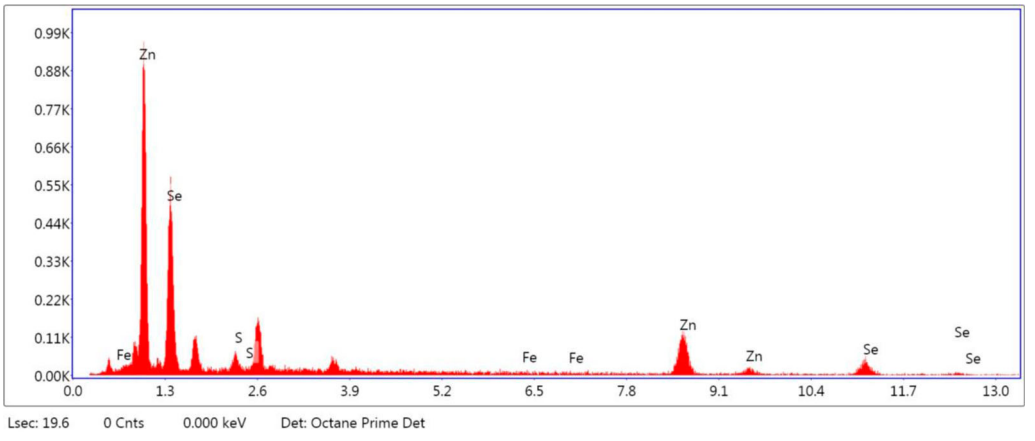

(d)

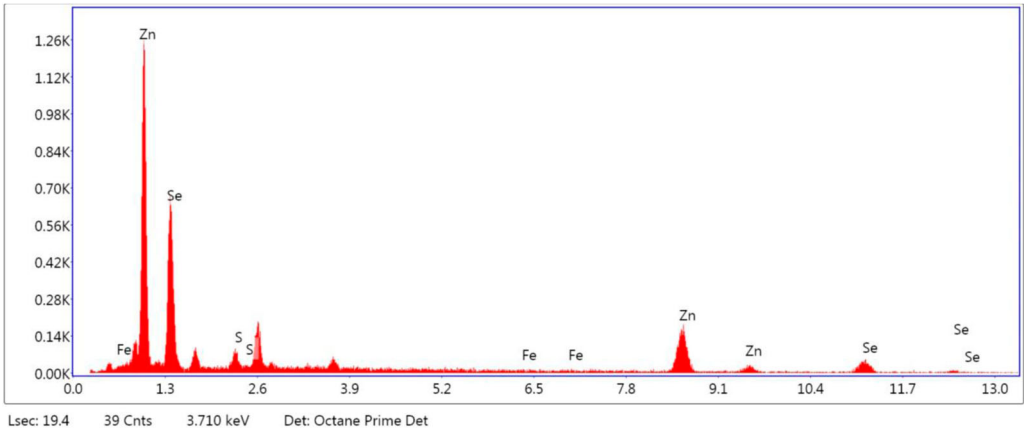

(e)

Figure 4 *Continued*

indirect transitions are 1/2, 2 and 3/2, respectively. For allowed direct transitions, Equation (6) can be rewritten as [7]

$$\alpha h\upsilon = A(h\upsilon - Eg)^{1/2} \tag{7}$$

It was observed that the thin films exhibited a high absorption coefficient ($\sim 10^4$ cm^{-1}). In order to find the optical bandgap of the thin films from the absorption spectra, graphs of $(\alpha h\upsilon)^2$ vs. $(h\upsilon)$ (i.e. Tauc's plots) were drawn as in Figure 5(b). It is possible to determine the exact optical bandgap by extrapolating the straight-line portion of the plot of $(\alpha h\upsilon)^2$ against $(h\upsilon)$ to the energy $(h\upsilon)$ axis at $(\alpha h\upsilon)^2 = 0$. The straight-line nature of the graph at the absorption band edge indicates the existence of a direct allowed-type transition between the valence and conduction bands. Figure 6 shows the variation of the optical bandgap energy with Fe doping concentration for the spray-deposited Fe-doped $ZnS_{0.2}Se_{0.8}$ thin films. The direct allowed bandgap increases with increasing Fe doping concentration from 2.98 eV (for undoped $ZnS_{0.2}Se_{0.8}$) up to 3.25 eV for 0.2 mol% Fe doping. It should be noted that the ionic radius of Zn^{2+} is 74 pm, which is greater than the 69 pm of the dopant Fe^{3+} ion [56]. In the above case, increase in ionic radius is responsible for the reduction of the particle size. However, when the Fe doping concentration is increased above 0.20 mol%, the bandgap drops to 2.81 eV (for an Fe doping concentration of 1.0 mol%). This indicates that the bandgap of the

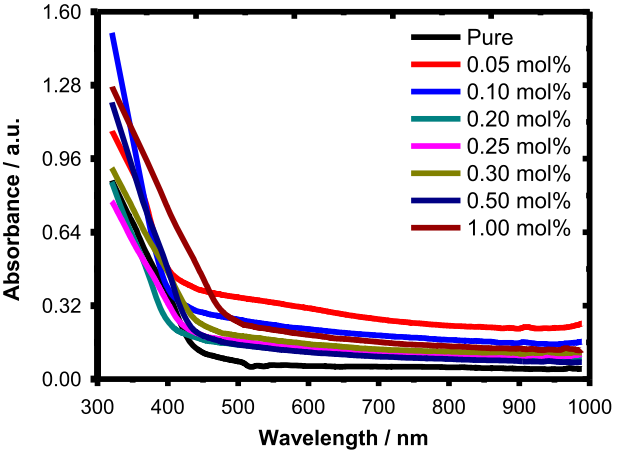

(a)

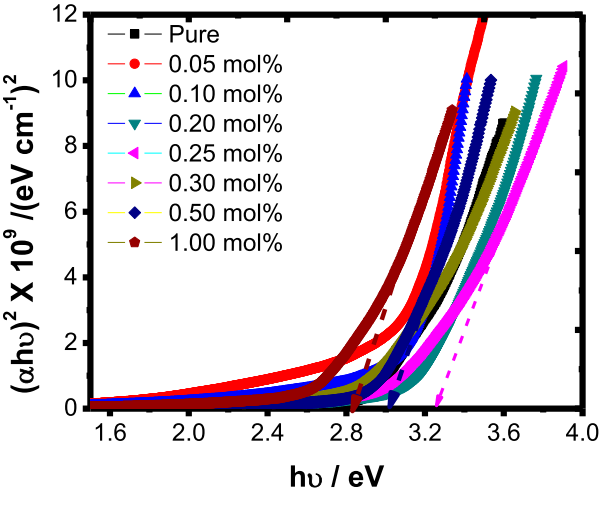

(b)

Figure 5. (a) Optical absorbance spectra and (b) plot of $(\alpha h\upsilon)^2$ vs. hυ for spray deposited Fe doped $ZnS_{0.2}Se_{0.8}$ thin films.

0.20 mol% Fe-doped $ZnS_{0.2}Se_{0.8}$ thin films is wider than those of the other Fe-doped $ZnS_{0.2}Se_{0.8}$ thin films.

3.5 Electrical resistivity studies

It is well known that the resistivity of a semiconducting materials falls with rising temperature as more free charge carriers (electrons and/or holes) are available per unit volume for conduction. This makes the temperature coefficient of semiconductors negative. The dark electrical resistivities (ρ) of the thin films were investigated using a simple, standard dc two-point probe technique in the temperature range 300–500 K using a Keithley Source Meter. Figure 7 shows the variation of log ρ v. the reciprocal of the absolute temperature ($1/T\times10^{-3}$) of the undoped and Fe-doped $ZnS_{0.2}Se_{0.8}$ thin films over a cooling cycle. This shows that the resistivity decreases with increasing temperature and confirms the semiconducting behavior of the Fe-doped $ZnS_{0.2}Se_{0.8}$ thin films. The calculated room temperature electrical resistivities were 8.51, 3.8, 1.45, 0.617, 1.07, 2.34, 16.6 and 33.1×10^5 Ω cm for undoped $ZnS_{0.2}Se_{0.8}$ and 0.05, 0.10, 0.20, 0.25, 0.30, 0.50 and 1.00 mol% Fe-doped $ZnS_{0.2}Se_{0.8}$ thin

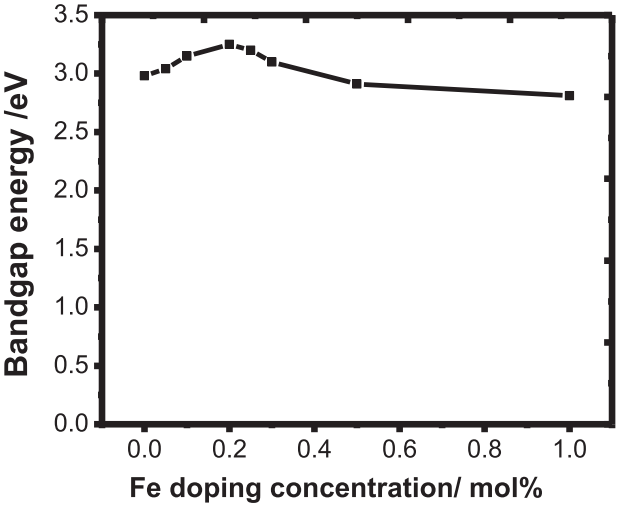

Figure 6. Variation of optical bandgap energy with Fe doping concentration for spray deposited Fe doped $ZnS_{0.2}Se_{0.8}$ thin films.

films, respectively. The observed low electrical resistivity for 0.20 mol% Fe-doped $ZnS_{0.2}Se_{0.8}$ is due to the homogeneous distribution of Fe^{3+} in the $ZnS_{0.2}Se_{0.8}$ lattice and its high ionic mobility [57]. Due to Fe^{3+} dopant the enhancement of grain size and decrease in boundary potential observed that increases not only carrier concentration but also mobility (as seen from Hall Effect measurement), resulting in a decrease in electrical resistivity up to 0.20 mol% Fe concentration [25, 58]. It is remarkable that the room temperature electrical resistivities fall noticeably with the incorporation of Fe^{3+} ions into the $ZnS_{0.2}Se_{0.8}$ crystal structure, attaining the lowest value of 0.617×10^{5} Ω cm at 0.20 mol% Fe^{3+} content.

The activation energies of all the Fe-doped $ZnS_{0.2}Se_{0.8}$ thin films were determined using the Arrhenius relation,

$$\rho = \rho_0 \exp\left(\frac{E_a}{kT}\right) \tag{8}$$

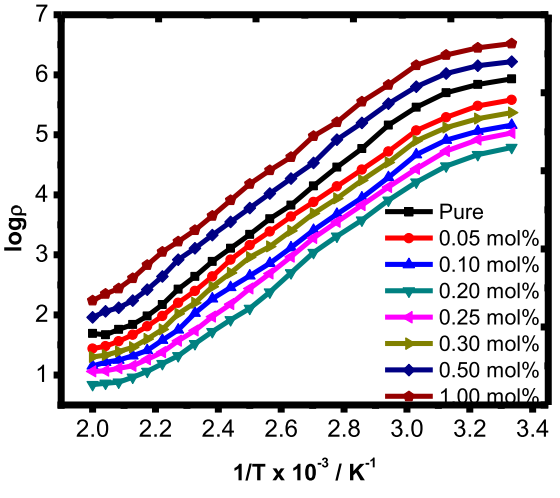

Figure 7. Variation of logρ vs. 1/T for spray deposited Fe doped $ZnS_{0.2}Se_{0.8}$ thin films.

Table 4. Optical and electrical properties of spray deposited of $ZnS_{0.2}Se_{0.8}$ and Fe-doped $ZnS_{0.2}Se_{0.8}$ thin films.

Doping Concentration (mol%)	Band gap E_g (eV)	Electrical resistivity (Ωcm)		Activation energy (eV)	
		300 K (× 10^5)	500 K (× 10^2)	L.T.	H.T.
Pure	2.98	8.51	48.98	0.07	0.11
0.05	3.04	3.80	27.55	0.07	0.11
0.10	3.15	1.45	14.13	0.14	0.11
0.20	3.25	0.617	6.92	0.06	0.10
0.25	3.20	1.07	11.48	0.15	0.11
0.30	3.10	2.34	19.96	0.11	0.13
0.50	2.91	16.6	91.21	0.13	0.16
1.00	2.81	33.1	173.78	0.12	0.19

In this equation, ρ and ρ_0 represent the resistivities, E_a is the activation energy, k is the Boltzmann constant and T is the absolute temperature in Kelvin. Table 4 lists the electrical resistivities and activation energies of the thin films at 300 and 500 K, respectively.

3.6 Hall Effect studies

The Hall Effect measurement is a valuable tool for analyzing the material characterization. The carrier concentration and mobility of the spray deposited Fe-doped $ZnS_{0.2}Se_{0.8}$ thin films are measured through Van-der Paw technique and are given in Table 5. It can be seen that, both undoped and Fe-doped $ZnS_{0.2}Se_{0.8}$ thin films have n-type conductivity. The carrier concentration and mobility of the $ZnS_{0.2}Se_{0.8}$ thin film increases with increase in Fe doping concentration up to 0.2 mol % and decreases with further increase in Fe doping concentration above 0.2 mol %. Similar doping concentration dependent behavior of ZnS and ZnSe thin films has been reported by Rao [59].

3.7 Thermoelectric power (TEP) studies

Amongst the several transport properties which describe the conduction process, TEP or Seebeck coefficient is the most beneficial parameter. In semiconductors, TEP measurements are relatively useful in examining the nature of charge carriers. Measurements of TEP were made on undoped and Fe-doped $ZnS_{0.2}Se_{0.8}$ thin films during the cooling cycles. Figure 8 displays the variation of the thermo-emf with temperature difference for the undoped and Fe-doped $ZnS_{0.2}Se_{0.8}$ thin films. It was found that the thermo-emf produced across the ends of Fe-doped $ZnS_{0.2}Se_{0.8}$ thin films were directly proportional to the temperature gradient maintained across the undoped and Fe-doped $ZnS_{0.2}Se_{0.8}$ thin films. The type of conductivity exhibited by Fe-doped $ZnS_{0.2}Se_{0.8}$ thin films was determined from the sign of the thermo-emf generated at the cold and hot end. The polarity of the thermally generated voltage at the hot end was positive

Table 5. Carrier concentration and mobility of spray deposited of $ZnS_{0.2}Se_{0.8}$ and Fe-doped $ZnS_{0.2}Se_{0.8}$ thin films.

Doping Concentration (mol%)	Sheet resistance Rs (Ω/□)	Carrier type	Carrier concentration (×10^{17} cm^{-3})	Carrier mobility (×10^{-4} cm^2/V-s)
Pure	30.95	n	0.46	1.61
0.05	13.57	n	0.95	1.74
0.10	5.09	n	2.45	1.76
0.20	2.10	n	5.96	1.80
0.25	3.54	n	3.30	1.77
0.30	7.52	n	1.82	1.47
0.50	51.71	n	0.27	1.39
1.00	100.30	n	0.14	1.38

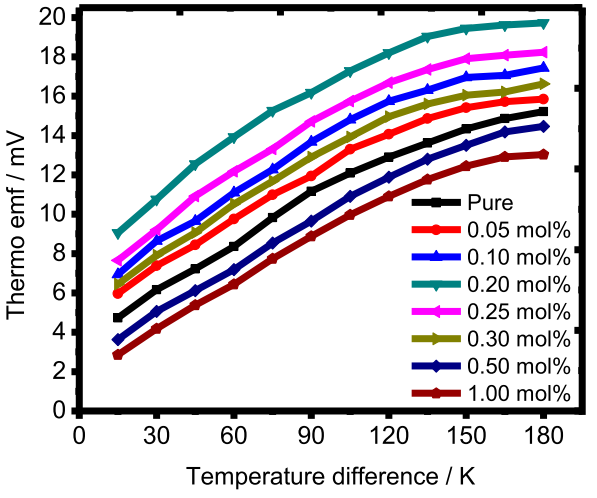

Figure 8. Plot of thermoemf vs. temperature difference for spray deposited Fe doped $ZnS_{0.2}Se_{0.8}$ thin films.

with respect to the cold end, showing that the nature of charge carriers in Fe-doped $ZnS_{0.2}Se_{0.8}$ thin films was n-type.

From Figure 8, it is witnessed that the thermo-emf is linearly dependent on temperature in the low-temperature region whereas it is weakly dependent or almost independent on temperature in the higher temperature region. The thermo-emf is doping dependent. As the Fe doping in $ZnS_{0.2}Se_{0.8}$ thin film increases, thermo-emf increases up to 0.20 mol% and decreases for further Fe doping in $ZnS_{0.2}Se_{0.8}$ thin films. The small change in the average grain size of the crystallites is responsible for the change in the TEP [60, 61].

4. Conclusions

Nanocrystalline undoped and Fe-doped $ZnS_{0.2}Se_{0.8}$ thin films with various Fe doping concentrations (0.05–1.00 mol%) were grown successfully onto well-cleaned soda lime glass substrates using the simple, convenient and cost-effective chemical spray pyrolysis technique. XRD revealed that the films had a polycrystalline zinc blende (cubic) crystal structure with preferential orientation along the (111) plane regardless of the Fe doping concentration. SEM shows a spherical-like structure with agglomeration of grains and a slight increase in the particle size with increasing Fe doping concentration. Energy-dispersive X-ray spectroscopy studies confirmed that Fe ions were successfully incorporated into the $ZnS_{0.2}Se_{0.8}$. The optical studies indicate direct bandgap energy in the range of 2.81–3.25 eV. There was a significant drop in the electrical resistivity (0.617×10^5 Ω cm) for 0.20 mol% Fe doping. The carrier concentration and mobility were observed to be 5.96×10^{17} cm^{-3} and 1.80×10^{-4} cm^2/V-s respectively for 0.20 mol% Fe-doped $ZnS_{0.2}Se_{0.8}$ thin films. The Hall Effect and TEP results showed that the electrical conductivity of the Fe-doped $ZnS_{0.2}Se_{0.8}$ thin films was of the n-type. Remarkable variations in the electrical resistivity and controlled direct bandgap of the Fe-doped $ZnS_{0.2}Se_{0.8}$ thin films were found. It is expected that spray-deposited Fe-doped $ZnS_{0.2}Se_{0.8}$ films with decreased electrical resistivity and controlled band gap, such as those studied in this work will be most promising for optoelectronic device applications.

Disclosure statement

No potential conflict of interest was reported by the author(s).

ORCID

Abhijit A. Yadav http://orcid.org/0000-0002-3486-4099

References

[1] Kocakülah G, Önsal G, Köysal O. Dielectric properties of CdSeS/ZnS quantum dots doped PMMA/LC composite structure. Ph Transit. 2019;92(10):907–915.
[2] Messaoudi O, Elgharbi S, Bougoffa A, et al. Annealing temperature investigation on electrodeposited Cu_2O properties. Ph Transit. 2020;93(10–11):1089–1099.
[3] Henry J, Daniel T, Balasubramanian V, et al. Electrical and optical properties of Sb-doped Cu_2Se thin films deposited by chemical bath deposition. Ph Transit. 2020;93(8):793–801.
[4] Messaoudi O, Mansouri M, Manai L, et al. Spectroscopic ellipsometry investigation and morphological characterization of electrodeposited Cu_2O thin films: annealing effect. Ph Transit. 2020;93(12):1171–1182.
[5] Jalalian-Larki B, Jamali-Sheini F, Yousefi R. Electrodeposition of In-doped SnSe nanoparticles films: correlation of physical characteristics with solar cell performance. Solid State Sci. 2020;108:106388.
[6] Salim HI. The effect of growth technique on the characteristic properties of CdS layers for solar cell applications. J Mater Sci: Mater Electron. 2020;31:4193–4207.
[7] Othman AA, Osman MA, Ali MA, et al. Sonochemically synthesized Ni-doped ZnS nanoparticles: structural, optical, and photocatalytic properties. J Mater Sci: Mater Electron. 2020;31:1752–1767.
[8] Mendil R, Ben Ayadi Z, Vázquez-Vázquez C, et al. A new procedure to synthesis of $ZnS_{1-x}Se_x$ nanoparticles by a facile solvothermal method. J Mater Sci: Mater Electron. 2018;29:10656–10662.
[9] Farazin J, Pirgholi-Givi G, Azizian-Kalandaragh Y. Wettability measurement, optical characteristics, and investigation of the quantum confinement effect of ZnS-scotch tape nanocomposite films prepared by successive ionic layer adsorption and reaction (SILAR) method. Physica B. 2019;564:94–103.
[10] Satoh S. Fiber multilayered ZnS position-sensitive neutron detector with high detection efficiency. Physica B. 2018;551:401–404.
[11] Venkata Subbaiah YP, Prathap P, Reddy KTR, et al. Growth and characterization of ZnS_xSe_{1-x} films deposited by close-spaced evaporation. J. Phys. D: Appl. Phys. 2007;40:3683–3688.
[12] Lin Y-C, Liu K-T, Hsieh T-P, et al. Improving Ga distribution and efficiency of flexible Cu(In,Ga)(S,Se) solar cell using CuGa:Na target route. Mater Sci Semicond Process. 2019;94:151–155.
[13] Ihanus J, Ritala M, Leskela M, et al. ALE growth of $ZnS_{1-x}Se_x$ thin films by substituting surface sulfur with elemental selenium. Appl Surf Sci. 1997;112:154–158.
[14] Liu J, Wei AX, Zhuang MX, et al. Investigation of the ZnS_xSe_{1-x} thin films prepared by chemical bath deposition. J Mater Sci: Mater Electron. 2013;24:1348–1353.
[15] Huang C-H, Yang C-H, Shieh Y-T, et al. Synthesis and properties of alloyed $Cd_xZn_{1-x}Se$ core and manganese-doped $Cd_xZn_{1-x}Se$/ZnS core/shell nanocrystals. J Alloy Comp. 2018;748:265–272.
[16] Zhang X, Meng D, Tang Z, et al. Preparation of radial ZnSe-CdS nano-heterojunctions through atomic layer deposition method and their optoelectronic applications. J Alloy Comp. 2019;777:102–108.
[17] He L, Yang L, Liu B, et al. One-pot synthesis of color-tunable copper doped zinc sulfide quantum dots for solid-state lighting devices. J Alloy Comp. 2019;787:537–542.
[18] Qiao F, Kang R, Liang Q, et al. Tunability in the optical and electronic properties of ZnSe microspheres via Ag and Mn doping. ACS Omega. 2019;4:12271–12277.
[19] Sharma K, Al-Kabbi AS, Saini GSS, et al. Indium doping induced modification of the structural, optical and electrical properties of nanocrystalline CdSe thin films. J Alloy Comp. 2013;564:42–48.
[20] Lohar GM, Shinde SK, Rath MC, et al. Structural, optical, photoluminescence, electrochemical, and photoelectrochemical properties of Fe doped ZnSe hexagonal nanorods. Mater Sci Semicond Process. 2014;26:548–554.
[21] Yellaiah G, Hadasa K, Nagabhushanam M. Growth, characterization, optical and vibrational properties of Sm^{3+} doped $Cd_{0.8}Zn_{0.2}S$ semiconductor compounds. J Crystal Growth. 2014;386:62–68.
[22] Saikia D, Raland RD, Borah JP. Influence of Fe doping on the structural, optical and magnetic properties of ZnS diluted magnetic semiconductor. Physica E. 2016;83:56–63.
[23] Siddiqui FY, Shaikh SU, Upadhye DS, et al. Investigation on the effect of copper doping on $CdS_{1-x}Se_x$ thin films. Ferroelectrics. 2017;518:153–162.
[24] Lohar GM, Jadhav ST, Dhaygude HD, et al. Studies of properties of Fe^{3+} doped ZnSe nanoparticles and hollow spheres for photoelectrochemical cell application. J Alloy Comp. 2015;653:22–31.
[25] Bhuse VM, Hankare PP, Sonandkar S. Structural, optical, electrical and photo-electrochemical studies on indium doped $Cd_{0.6}Hg_{0.4}Se$ thin films. Mater Chem Phys. 2007;101:303–309.
[26] Chukavin AI, Valeev RG, Zubavichus YV, et al. Study of the $ZnS_xSe_{1-x}@Al_2O_3$ nanostructures by X-ray diffraction and EXAFS spectroscopy. J Struct Chem. 2017;58:1236–1244.

[27] Bhattacharyya S, Ghosh B, Das S. Air annealing induced growth of self-assembled ultra-long ZnS microwire: structural and photoluminescence studies. Mater Sci Semicond Process. 2018;76:65–72.
[28] Ganguly A, Chaudhuri S, Pal AK. Synthesis of ZnS_xSe_{1-x} nanocrystalline thin films. J. Phys. D: Appl. Phys. 2001;34:506–513.
[29] Da-ke S, Sou IK, Gao-Rong H, et al. Polycrystalline ZnS_xSe_{1-x} thin films deposited on ITO glass by MBE. J. Zhejiang Univ. Sci. A. 2003;4(2):131–135.
[30] Kumar V, Sharma TP. Structural and optical properties of sintered ZnS_xSe_{1-x} films. Opt Mater. 1998;10:253–256.
[31] Dhanemozhi C, John R, Murali KR. Synthesis and characterization of ZnS_xSe_{1-x} films using brush plating technique. Materials Today: Proceedings. 2017;4:5185–5189.
[32] Zhang T, Wang Y, Pan Z. Synthesis and characterization of Cu-/In-co-doped ZnS_xSe_{1-x} with tunable band-gaps as high near-infrared reflective color pigments. Ceram Internat. 2018;44:18851–18862.
[33] Popa M. The optical properties of ZnS_xSe_{1-x} thin films deposited by the quasi-closed volume technique. Rom Rep Phys. 2016;68:1495–1505.
[34] Agawane GL, Seung WS, Vanalakar SA, et al. Non-toxic novel route synthesis and characterization of nanocrystalline ZnS_xSe_{1-x} thin films with tunable band gap characteristics. Mater Res Bull. 2014;55:106–113.
[35] Alghamdi Y. Composition and band Gap controlled AACVD of ZnSe and ZnS_xSe_{1-x} thin films using novel single Source precursors. Mater Sci Appl. 2017;8:726–737.
[36] Ramakrishna Reddy KT, Subbaiah YV, Reddy TBS, et al. Pyrolytic spray deposition of ZnS_xSe_{1-x} layers for photovoltaic applications. Thin Solid Films. 2003;431-432:340–343.
[37] Perednis D, Gauckler LJ. Thin Film Deposition using spray pyrolysis. J Electroceramics. 2005;14:103–111.
[38] Benramdane N, Murad WA, Misho RH, et al. A chemical method for the preparation of thin films of CdO and ZnO. Mater Chem Phy. 1997;48:119–123.
[39] Patil PS. Review versatility of chemical spray pyrolysis technique. Mater Chem Phy. 1999;59:185–198.
[40] Chopra KL, Das SR. Thin Film Deposition techniques. Thin film solar cells. Chapter. 1983;5:195–273.
[41] Patil NM, Nilange SG, Yadav AA. Growth and characterization of ZnS_xSe_{1-x} thin films deposited by spray pyrolysis. Thin Solid Films. 2018;664:19–26.
[42] Patil NM, Nilange SG, Yadav AA. Properties of spray deposited ZnSxSe1-x thin films for photoelectrochemical solar cell application. J Mater Sci: Mater in Electron. 2019;30:1647–1653.
[43] Yadav AA, Masumdar EU. Preparation and characterization of indium doped $CdS_{0.2}Se_{0.8}$ thin films by spray pyrolysis. Mater Res Bull. 2010;45:1455–1459.
[44] Lohar GM, Dhaygude HD, Patil RA, et al. Studies of properties of Fe^{2+} doped ZnSe nano-needles for photoelectrochemical cell application. J Mater Sci: Mater Electron. 2015;26:8904–8914.
[45] Poornaprakash B, Amaranatha Reddy D, Murali G, et al. Defect induced paramagnetism in lightly doped ZnS: Fe nanoparticles. Physica E. 2015;73:63–68.
[46] Yadav K, Dwivedi Y, Jaggi N. Structural and optical properties of Ni doped ZnSe nanoparticles. J Lumin. 2015;158:181–187.
[47] Khalate SA, Kate RS, Pathan HM, et al. Structural and electrochemical properties of spray deposited molybdenum trioxide (α-MoO_3) thin films. J Solid State Electrochem. 2017;21:2737–2746.
[48] Bakiyaraj G, Dhanasekaran R. Synthesis and characterization of flower-like ZnSe nanostructured thin films by chemical bath deposition (CBD) method. Appl Nanosci. 2013;3:125–131.
[49] Khan S, Han JS, Lee SY, et al. ZnS nano-spheres formed by the aggregation of small crystallites and their photocatalytic degradation of eosin B. Chin. J. Chem. 2017;35:159–164.
[50] Theivasanthi T, Kartheeswari N, Alagar M. Chemical precipitation synthesis of ferric chloride doped zinc sulphide nanoparticles and their characterization studies. Chem Sci Trans. 2013;2:497–507.
[51] Khani O, Rajabi HR, Yousefi MH, et al. Synthesis and characterizations of ultra-small ZnS and $Zn_{(1-x)}Fe_xS$ quantum dots in aqueous media and spectroscopic study of their interactions with bovine serum albumin. Spectrochim Acta, Part A. 2011;79:361–369.
[52] Rajabi HR, Khani O, Shamsipur M, et al. High-performance pure and Fe^{3+} ion doped ZnS quantum dots as green nanophotocatalysts for the removal of malachite green under UV-light irradiation. J Hazardous Mater. 2013;250–251:370–378.
[53] Lohar GM, Jadhav ST, Relekar BP, et al. Electrochemically synthesized 1D and 3D hybrid Fe^{3+} doped ZnSe dandelions for photoelectrochemical cell application. Optik (Stuttg). 2018;158:53–63.
[54] Thanikaikarasana S, Sundarama K, Mahalingama T, et al. Electrodeposition and characterization of Fe doped CdSe thin films from aqueous solution. Mater Sci Engg B. 2010;174:242–248.
[55] Rajesh Kumar T, Prabukanthan P, Harichandran G, et al. Comparative study of structural, optical and electrical properties of electrochemically deposited Eu, Sm and Gd doped ZnSe thin films. J Mater Sci Mater Elect. 2018;29:5638–5648.
[56] Rajesh Kumar T, Prabukanthan P, Harichandran G, et al. Physicochemical and electrochemical properties of Gd^{3+} doped ZnSe thin films fabricated by single-step electrochemical deposition process. J Solid State Electrochem. 2018;22:1197–1207.

[57] Shyniya CR, Amarsingh Bhabu K, Rajasekaran TR. Enhanced electrochemical behavior of novel acceptor doped titanium dioxide catalysts for photocatalytic applications. J Mater Sci: Mater Electron. 2017;28:6959–6970.
[58] Garadkar KM, Hankare PP, Patil RK. Effect of indium doping on structural, optical and electrical properties of $Cd_{0.95}Hg_{0.05}S$ thin films. Mater Chem Phy. 1999;58:64–70.
[59] Rao GK. Doping ZnS and ZnSe thin films with bismuth: A comparison between sandwiching technique and nano-particle incorporation. Mater Sci Semicond Process. 2014;26:137–143.
[60] Patil PS, Mujawar SH, Inamdar AI, et al. Structural, electrical and optical properties of TiO_2 doped WO_3 thin films. Appl Surf Sci. 2005;252:1643–1650.
[61] Nasiraei R, Fadavieslam MR, Azimi-Juybari H. Structural, photoconductive, thermoelectric and activation energy measurements of V-doped transparent conductive SnO_2 films fabricated by spray pyrolysis technique. Pramana-J. Phys. 2016;87:30–39.